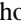



# Voltage-controlled magnetic anisotropy in an ultrathin nickel film studied by *operando* x-ray magnetic circular dichroism spectroscopy

Risa Miyakaze,<sup>1</sup> Shoya Sakamoto <sup>2</sup>, Takeshi Kawabe,<sup>1</sup> Takuya Tsukahara,<sup>1</sup> Yoshinori Kotani <sup>3</sup>, Kentaro Toyoki,<sup>3</sup> Tetsuya Nakamura,<sup>3</sup> Minoru Goto,<sup>1</sup> Yoshishige Suzuki,<sup>1</sup> and Shinji Miwa <sup>1,2,4,\*</sup>

<sup>1</sup>Graduate School of Engineering Science, Osaka University, Osaka 560-8531, Japan

<sup>2</sup>The Institute for Solid State Physics, The University of Tokyo, Chiba 277-8581, Japan

<sup>3</sup>Japan Synchrotron Radiation Research Institute (JASRI), Hyogo 679-5198, Japan

<sup>4</sup>Trans-scale Quantum Science Institute, The University of Tokyo, Tokyo 113-0033, Japan



(Received 21 April 2020; revised 26 June 2020; accepted 29 June 2020; published 13 July 2020)

Voltage-controlled magnetic anisotropy (VCMA) in an atomically thin Ni film placed at an epitaxial Fe-MgO interface has been studied. We characterize the VCMA by employing Fe/Ni/MgO-based magnetic tunnel junction. Moreover, we conduct x-ray magnetic circular dichroism (XMCD) spectroscopy around Ni absorption edges under an external voltage application to the tunnel junction device. This *operando* XMCD spectroscopy demonstrates voltage-induced changes of orbital and effective spin magnetic moments of Ni. As compared with the previous study, where *operando* XMCD spectroscopy was performed on an atomically thin Co film, we find that the magnitude of the VCMA effect in Ni and Co is proportional to the voltage-induced change of the orbital magnetic moment. This study would lead to a comprehensive understanding of how an electric field affects interfacial magnetism in ferromagnetic metals.

DOI: [10.1103/PhysRevB.102.014419](https://doi.org/10.1103/PhysRevB.102.014419)

## I. INTRODUCTION

Perpendicular magnetic anisotropy (PMA) in ferromagnetic ultrathin metals [1–6] has been intensively studied for high-density magnetic recording disks and magnetic random-access memory (MRAM) devices. Moreover, control of the PMA energy by an external voltage, that is, voltage-controlled magnetic anisotropy (VCMA), has been studied intensively due to its potential for the operation technology of the MRAM [5–10].

For a ferromagnetic metal, there are two mechanisms to explain the PMA and the VCMA. One is the orbital magnetic-moment mechanism, also known as the Bruno model, where the orbital-magnetic-moment anisotropy is proportional to the PMA energy [2,4]. The other is the quadrupole mechanism, where the PMA energy originates from an anisotropic spin distribution of the 3*d* electrons through the spin-orbit interaction [3,6,11]. These two mechanisms are derived from the perturbation theory for the second-order spin-orbit interaction energy. The orbital magnetic-moment (quadrupole) mechanism corresponds to the spin-conserved (spin-flip) virtual excitation process. In general, it is believed that the orbital magnetic-moment mechanism explains the PMA and the VCMA in 3*d* transition metals. Actually, it has been theoretically found that the VCMA originates from the modulation of the 3*d* orbitals [12–16]. Moreover, the voltage-induced change of the orbital magnetic moment, which is relevant to the PMA energy, of Co has been recently reported [17].

Fe and Ni are similar ferromagnetic 3*d* transition metals to Co. For Fe, the application of the Bruno model is not obvious

because the majority-spin band of Fe is not completely occupied. However, this is not the case for Ni. Similar to Co, the majority-spin band of Ni is believed to be fully occupied, and the minority-spin band should have a dominant contribution to the PMA and the VCMA. In this regard, studying Ni in terms of the voltage-induced changes of PMA energy and magnetic moments would be an important milestone to understand the VCMA effect. Here we report on the VCMA of an ultrathin Ni layer placed at an interface between Fe and MgO and its voltage-induced changes of the orbital magnetic moment. These are characterized by using spin-torque-induced ferromagnetic resonance (FMR) [18–20] and *operando* x-ray-absorption spectroscopy in tunnel junctions [6,11,17,21–24], respectively.

## II. EXPERIMENT

First, Fe/Ni/MgO-based magnetic tunnel junctions, schematically shown in Fig. 1(a), were prepared. This was used to characterize the VCMA in an ultrathin Ni film. A multilayer consists of the following structure: MgO(001) substrate/MgO buffer (5 nm)/V (30 nm)/Fe (0.3 nm)/Ni (0–0.14 nm)/MgO barrier (1.4 nm)/Fe (10 nm)/Au (5 nm). All of the layers were epitaxially grown using the molecular-beam epitaxy method under an ultrahigh vacuum at room temperature. The MgO substrate and the V layer was annealed at 800 °C for 10 min and at 500 °C for 30 min, respectively. Because of the MgO buffer, carbon diffusion from the MgO substrate surface is reduced [25]. The V layer was employed to induce PMA energy in the system [26,27]. As shown in Fig. 1(b), clear streak patterns were observed in the reflection high-energy electron-diffraction images guaranteeing the formation of epitaxial and flat interfaces between each

\*miwa@issp.u-tokyo.ac.jp

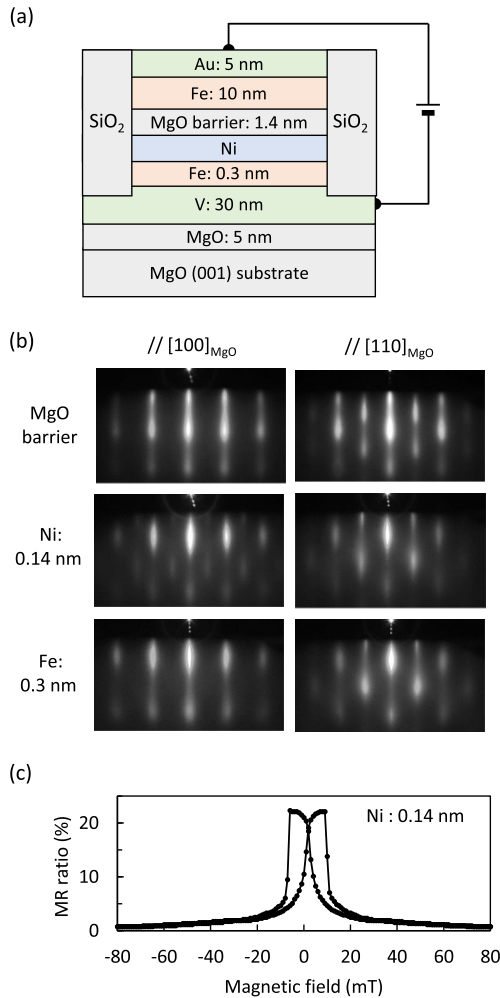


FIG. 1. (a),(b) Schematic illustration of the device structure to characterize voltage-controlled magnetic anisotropy (VCMA) in Ni. (b) *In situ* reflection high-energy electron-diffraction images of each layer surface. (c) A typical magnetoresistance. Magnetic field was applied parallel to the film plane in [100] ([110]) direction of Fe (MgO).

layer [28]. The 0.14-nm Ni corresponds to a monatomic layer of Ni. Magnetic tunnel junctions having  $2 \times 5 \mu\text{m}^2$  junction size were fabricated from the multilayer. Figure 1(c) shows a typical result of tunneling magnetoresistance measurements. Magnetic field was applied parallel to the film plane in [100] ([110]) direction of Fe (MgO).

Next, similar tunnel junctions with a different design have been prepared. This was used to characterize the change of XMCD induced by an external voltage. The XMCD spectra were measured using a four-element silicon drift detector (SDD) with the partial fluorescence yield (PFY) method. Figure 2(a) shows a schematic of the device structure. The multilayer consists of the following structure: MgO(001) substrate/MgO buffer (5 nm)/V (30 nm)/Fe (0.3 nm)/Ni (0.14 nm)/MgO barrier (2 nm). After taking out the multilayer from the vacuum, 5-nm-SiO<sub>2</sub>, 2-nm-Cr, and 5-nm-Au layers were deposited. An 80- $\mu\text{m}$ -diameter tunnel junction was fabricated from the multilayer. Finally a similar multilayer structure without a top SiO<sub>2</sub>/Cr/Au: MgO substrate/MgO buffer

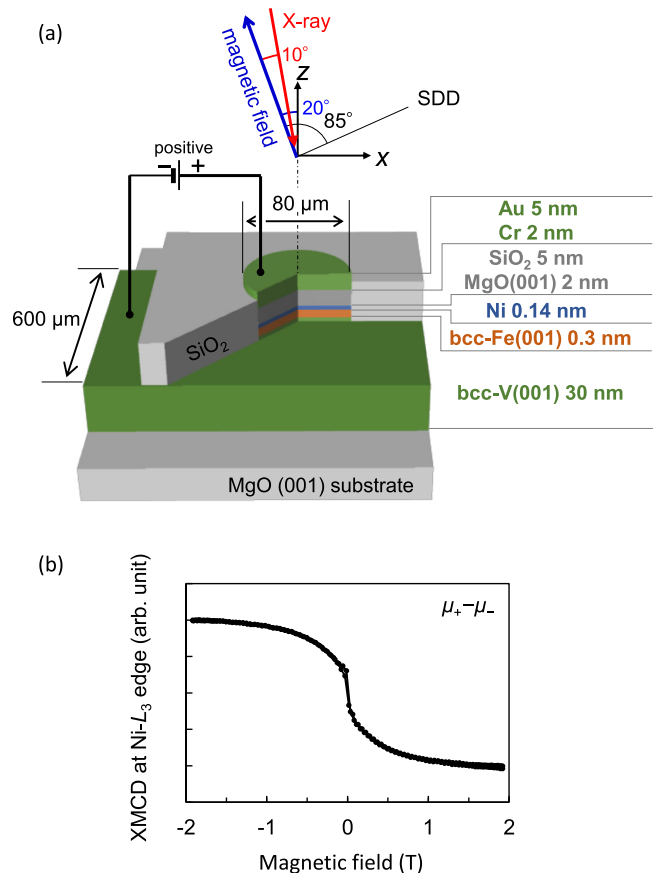


FIG. 2. (a) Schematic of the experimental design for *operando* x-ray magnetic circular dichroism (XMCD) spectroscopy. An external voltage was applied to the Ni layer via a MgO/SiO<sub>2</sub> dielectric. The XMCD spectroscopy were performed using the partial fluorescence yield (PFY) method with a silicon drift detector (SDD). (b) Magnetization hysteresis curve measured by XMCD at the Ni-L<sub>3</sub> edge (853.0 eV).

(5 nm)/V (30 nm)/Fe (0.3 nm)/Ni (0.14 nm)/MgO (2 nm) was prepared. This was used to measure XMCD spectra with the total electron yield (TEY) method.

The soft x-ray beamline (BL25SU, SPring-8) was employed for conducting the XMCD spectroscopy. The experimental conditions are reported elsewhere [17,29,30]. The x-ray absorption was recorded with right ( $\mu_+$ ) and left ( $\mu_-$ ) helicities at room temperature. Influence of the self-absorption effects due to the PFY method was calibrated by employing the spectra measured with the TEY method. The TEY method should be less affected by the self-absorption [31]. Figure 2(b) shows the magnetization hysteresis curve, which was collected using the XMCD at the Ni-L<sub>3</sub> edge (853.0 eV) with the PFY method. The magnetization of the Fe/Ni layer is saturated under a magnetic field of 1.9 T, where XMCD spectroscopy as mentioned below was conducted.

The magnetic moments in the V/Fe (0.3 nm)/Ni (0.14 nm)/MgO (2 nm) are characterized by applying the sum rules [32,33] to the XMCD spectra measured with the TEY method. Figure 3(a) represents the x-ray absorption and XMCD spectra at the L<sub>3</sub> and L<sub>2</sub> edges of Ni. A magnetic field of  $\pm 1.9$  T was applied to saturate the magnetization of

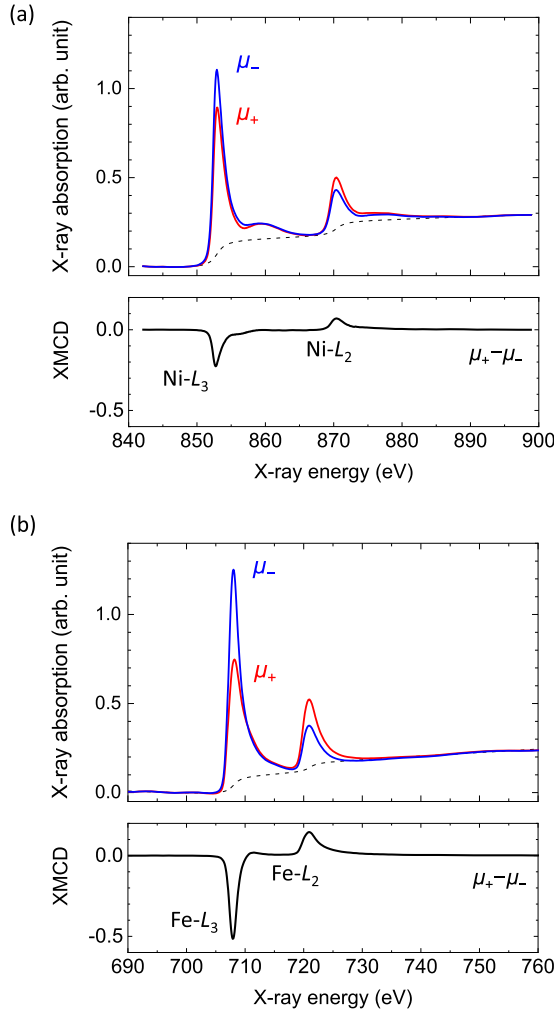


FIG. 3. (a) X-ray absorption and XMCD spectra of Ni. (b) X-ray absorption and XMCD spectra of Fe. These data are obtained using the TEY method.

the Fe/Ni layer. A linear function was subtracted from each x-ray-absorption spectrum. The dashed line is a background consisting of a double step function and a linear function, which is used for the sum-rule analysis. Nonmagnetic backgrounds were canceled by averaging the spectra measured for the reversed magnetic field. Figure 3(b) represents the x-ray-absorption and XMCD spectra at the  $L_3$  and  $L_2$  edges of Fe. The orbital magnetic moment ( $m_L$ ) is estimated to be  $0.07 \mu_B$  ( $0.12 \mu_B$ ) for Ni (Fe). Here  $\mu_B$  is the Bohr magneton. The effective spin magnetic moment ( $m_S - 7m_T$ ), where  $m_S$  and  $m_T$  denote respectively spin magnetic moment and magnetic dipole  $T_z$  term, is estimated to be  $0.41 \mu_B$  ( $1.79 \mu_B$ ) for Ni (Fe). For the sum-rule analysis, the numbers of  $3d$  holes of Ni and Fe were assumed to be 1.45 and 3.39, respectively [34,35].

### III. RESULTS AND DISCUSSION

#### A. Spin-torque FMR to characterize the VCMA effect of Ni

A VCMA coefficient of the Fe/Ni/MgO system was measured using the voltage-induced resonant field shift. We define

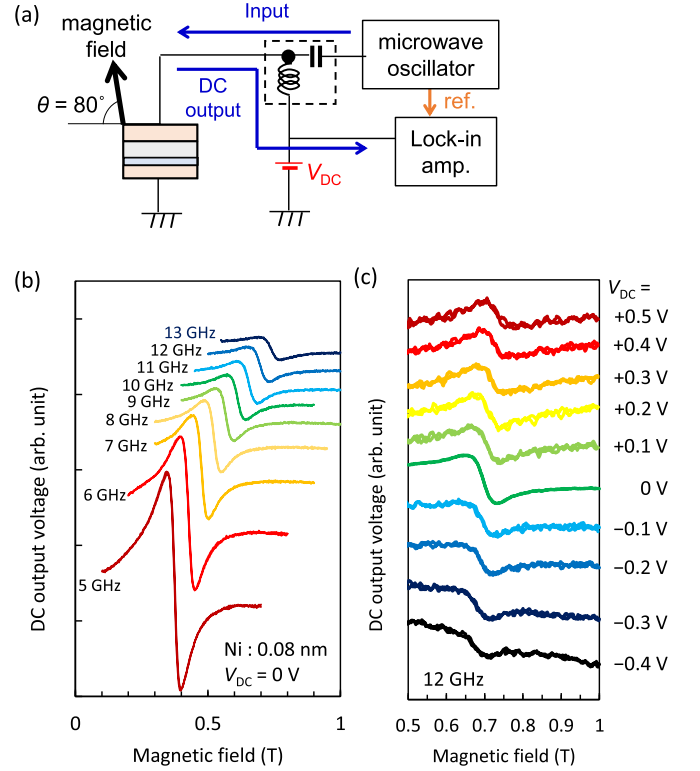


FIG. 4. (a) Schematic illustration of the measurement setup for VCMA-induced spin-torque ferromagnetic resonance (FMR). (b) Typical spectra of an Fe(0.3 nm)/Ni(0.08 nm)/MgO device under various input frequencies. (c) Typical spectra under DC bias ( $V_{DC}$ ). Input frequency was 12 GHz.

the VCMA coefficient as the PMA energy ( $\text{mJ}/\text{m}^2$ ) divided by an electric field ( $\text{V}/\text{m}$ ) in the MgO barrier. Figure 4(a) shows an experimental design. The magnetic tunnel junction in Fig. 1(a) is employed. The FMR of Fe/Ni is characterized using the VCMA-induced spin-torque FMR [20]. Figures 4(b) and 4(c) show typical FMR spectra recorded under various input current frequency ( $f$ ) and DC bias voltage ( $V_{DC}$ ), respectively.

Figure 5(a) shows the input current frequency as a function of the resonant field ( $H_{FMR}$ ). From an intercept of each linear fit in Fig. 5(a), the demagnetization field ( $H_d$ ) is estimated as shown in Fig. 5(b). We used the following equation:

$$f = -\frac{\gamma_0}{2\pi} \sqrt{(H_{FMR} - H_d \sin^2 \theta)(H_{FMR} + H_d \cos 2\theta)} \approx -\frac{\gamma_0}{2\pi} (H_{FMR} - H_d). \quad (1)$$

$\gamma_0 (< 0)$  is the gyromagnetic ratio. A VCMA coefficient ( $\xi$ ) can be derived from the changes in the demagnetization field ( $\delta H_d$ ) induced by the DC bias voltage [Fig. 5(c)] as

$$\xi = -\frac{1}{2} \mu_0 \delta H_d (M_{S,Fe} t_{Fe} + M_{S,Ni} t_{Ni}) \left( \frac{V_{DC}}{t_{MgO}} \right)^{-1}. \quad (2)$$

$M_S$  and  $t$  are the saturation magnetization and the layer thickness, respectively. The obtained VCMA coefficient is shown in Fig. 5(d). The VCMA coefficient decreases when the Ni layer is inserted. For the Fe/Ni(0.14 nm)/MgO system, where

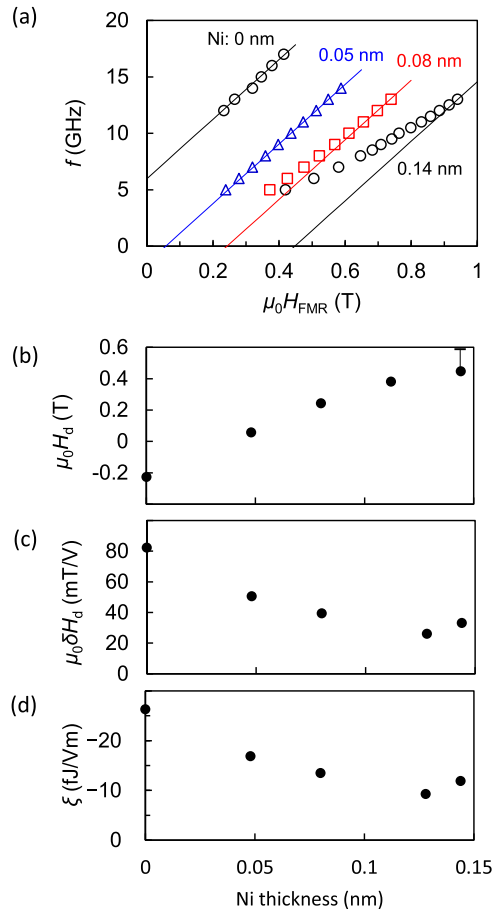


FIG. 5. (a) Input current frequency ( $f$ ) as a function of resonant field ( $H_{\text{FMR}}$ ). (b) Demagnetizing field ( $H_d$ ) determined from an intercept of each linear fit in panel (a). (c) Changes of the demagnetizing field ( $\delta H_d$ ) induced by DC bias voltage. (d) VCMA coefficient ( $\xi$ ).

Ni thickness corresponds to a monatomic layer, the VCMA coefficient is  $-14$  fJ/Vm, which is about half as large as that of Fe(0.3 nm)/MgO ( $-26$  fJ/Vm). The significant difference of the VCMA coefficients between Fe/MgO and Fe/Ni/MgO strongly suggests that the Ni/MgO interface dominates the VCMA in the Fe/Ni/MgO.

### B. Operando XMCD spectroscopy of Ni

In the Fe/Ni/MgO system, Fe/Ni ferromagnetic bilayer is employed. However, because the VCMA effect is dominated by the monatomic layer at the interface with MgO [11], we focus on Ni for the *operando* XMCD spectroscopy. Figures 6(a) and 6(b) show the results of the x-ray-absorption spectroscopy around the  $L_3$  and  $L_2$  edges of Ni using the PFY method, respectively. To direct the magnetization of the Fe/Ni layer the measurements were conducted under magnetic fields of  $\pm 1.9$  T [Fig. 2(b)].

Figures 7(a) and 7(b) show the voltage-induced changes of the XMCD signals. Peak heights of the Ni absorption edges, namely Ni- $L_3$  (853.0 eV) and - $L_2$  (870.6 eV), were collected with the PFY method. External magnetic fields of  $\pm 1.9$  T was applied during the measurements. Here,  $\pm 1.5$ -V voltage corresponds to  $\pm 0.1$ -V/nm electric field in the MgO barrier

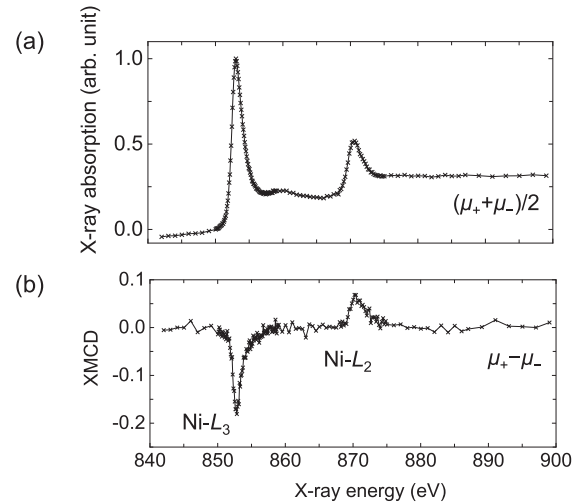


FIG. 6. (a) Polarization-averaged x-ray absorption ( $(\mu_+ + \mu_-)/2$ ) and (b) its XMCD ( $\mu_+ - \mu_-$ ) spectra obtained using the PFY method around the Ni-absorption edge. An external magnetic field of  $\pm 1.9$  T was applied to saturate the magnetization of the Fe/Ni layer in the magnetic field direction.

from the capacitance model [8]. In our definition, the positive voltage induces electrons at the interface between Ni and MgO. In Figs. 7(a) and 7(b), the error bars are not the accuracy errors but the errors accounting for the relative changes induced by the voltage, i.e., precision errors. Although the changes are relatively small as compared to the previous study using Co [17], similar changes were also observed at the Ni- $L_2$  and - $L_3$  absorption edges.

Figures 7(c) and 7(d) show the voltage-induced changes of the magnetic moments in Ni estimating with sum-rule analysis [32,33]. In the estimation, we assumed that the XMCD

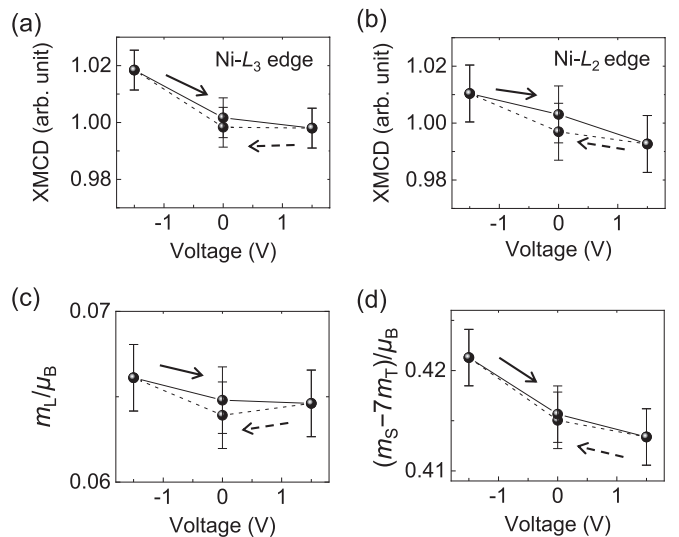


FIG. 7. (a),(b) Voltage-induced changes in the XMCD intensities at the Ni- $L_3$  (853.0 eV) and Ni- $L_2$  (870.6 eV) edges. (c),(d) Voltage-induced changes in the orbital magnetic moment ( $m_L$ ) and effective spin magnetic moment ( $m_S - 7m_T$ ) of Ni. A negative bias voltage, which accumulates holes at the interface between Ni and MgO, increases both the  $m_L$  and  $m_S - 7m_T$ .

integrals at the  $L_2$  and  $L_3$  edges of Ni, collected with TEY [Fig. 3(a)], were proportional to their peak heights [Figs. 7(a) and 7(b)]. An external voltage may change the  $3d$  holes of Ni, where the hole number is proportional to the white line intensities of the x-ray absorption, but this does not affect the results from sum-rule analysis. From Fig. 7(c), we can see that the orbital magnetic moment under a voltage application of  $-1.5$  V is slightly larger than that measured with  $+1.5$  V. Our experiment demonstrates that the orbital-magnetic-moment change of  $(0.0015 \pm 0.0020)\mu_B$  was induced by an external voltage  $\pm 1.5$  V/nm. Figure 7(d) shows the voltage-induced change in the effective spin magnetic moment ( $m_S - 7m_T$ ). As confirmed in Fig. 7(c) for the orbital magnetic moment, the effective spin magnetic moment in Ni is larger at a negative voltage. The significant modulation of the effective spin magnetic moment by voltage might be attributed to the modulation of the magnetic dipole  $T_z$  term ( $m_T$ ) [11,17].

To discuss the PMA energy, the second-order perturbation of the spin-orbit interaction energy is useful [6,36]:

$$\begin{aligned} \Delta E \approx & -\frac{1}{4} \frac{\lambda'}{\hbar} (\langle \Delta L_{\downarrow\downarrow} \rangle - \langle \Delta L_{\uparrow\uparrow} \rangle) \\ & + \frac{7}{2} \frac{\lambda'}{\hbar} (\langle \Delta T'_{\uparrow\uparrow} \rangle + \langle \Delta T'_{\downarrow\downarrow} \rangle). \end{aligned} \quad (3)$$

Here  $\lambda'$  is the effective spin-orbit interaction coefficient.  $L$  and  $T'$  are the orbital angular momentum and part of the magnetic-dipole operator, respectively.  $\langle \Delta L \rangle$  and  $\langle \Delta T' \rangle$  express  $\langle L_z \rangle - \langle L_x \rangle$  and  $\langle T'_z \rangle - \langle T'_x \rangle$ , respectively.  $\langle L_z \rangle (\langle T'_z \rangle)$  and  $\langle L_x \rangle (\langle T'_x \rangle)$  are the orbital angular momentum (magnetic dipole operator) for perpendicular and in-plane magnetizations, respectively. Here,  $\uparrow(\downarrow)$  denotes the contribution from the majority (minority) spin band. In Eq. (3), the first term is the PMA energy strongly correlated to the orbital angular momentum. When the majority spin band is occupied,  $\langle \Delta L_{\uparrow\uparrow} \rangle$  can be neglected. Then, the PMA energy can be proportional to anisotropy of the orbital magnetic moment from XMCD measurements,

$$\Delta E \approx \frac{\lambda'}{4\mu_B} \Delta m_L. \quad (4)$$

Equation (4) is same as the model proposed by Bruno [2,4]. Here, the majority spin band of Ni is believed to be almost

fully occupied, and therefore, the terms related to majority spin band ( $\uparrow$ ) can be neglected.

Here we compare the present results on Ni displayed in Fig. 7(c) with the previous study on Co [17]. The VCMA coefficient of Ni ( $-14$  fJ/V m) is  $\sim 17\%$  of that of Co ( $-82$  fJ/V m). Moreover, the induced changes of the orbital magnetic moment of Ni ( $0.008\mu_B$  per 1 V/nm) is  $\sim 16\%$  of that of Co ( $0.051\mu_B$  per 1 V/nm). Although the changes of the orbital magnetic moment are comparable to the error bars for the case of Ni, interestingly, the ratio between the VCMA coefficients of Ni and Co is almost the same as that of the changes of the orbital magnetic moment. The results show that the VCMA in Ni is consistent with the *orbital magnetic moment mechanism*. More precisely, PMA energy is not proportional to the orbital magnetic moment under perpendicular magnetization but to the orbital-magnetic-moment anisotropy. However, the trend of the voltage-induced changes of the orbital magnetic moment and its anisotropy are similar [17], and therefore, we believe that the aforementioned discussion is qualitatively correct.

#### IV. CONCLUSION

In this study, the VCMA effect in Ni has been experimentally characterized using spin-torque FMR and *operando* XMCD spectroscopy, respectively. Given that the orbital magnetic-moment mechanism is applicable to the  $3d$ -transition metals, we find that the voltage-induced changes of the orbital magnetic moment is consistent with the VCMA effect in Ni. This paper provides deep insight into the voltage control of interfacial magnetism.

#### ACKNOWLEDGMENTS

Part of this work was supported by JSPS KAKENHI (Grants No. JP18H03880 and No. JP20K15158), the Asahi Glass Foundation, ImPACT program, and the Spintronics Research Network of Japan (Spin-RNJ). The XMCD measurements were performed in SPring-8 with the approval of the Japan Synchrotron Radiation Research Institute (Proposals No. 2017A1201, No. 2017B1003, and No. 2017B1969).

- 
- [1] P. F. Carcia, A. D. Meinhaldt, and A. Suna, Perpendicular magnetic anisotropy in Pd/Co thin film layered structures, *Appl. Phys. Lett.* **47**, 178 (1985).
- [2] P. Bruno, Tight-binding approach to the orbital magnetic moment and magnetocrystalline anisotropy of transition-metal monolayers, *Phys. Rev. B* **39**, 865 (1989).
- [3] G. van der Laan, Microscopic origin of magnetocrystalline anisotropy in transition metal thin films, *J. Phys.: Condens. Matter* **10**, 3239 (1998).
- [4] J. Stöhr, Exploring the microscopic origin of magnetic anisotropies with X-ray magnetic circular dichroism (XMCD) spectroscopy, *J. Magn. Magn. Mater.* **200**, 470 (1999).
- [5] B. Dieny and M. Chshiev, Perpendicular magnetic anisotropy at transition metal/oxide interfaces and applications, *Rev. Mod. Phys.* **89**, 025008 (2017).
- [6] S. Miwa, M. Suzuki, M. Tsujikawa, T. Nozaki, T. Nakamura, M. Shirai, S. Yuasa, and Y. Suzuki, Perpendicular magnetic anisotropy and its electric-field-induced change at metal-dielectric interfaces, *J. Phys. D: Appl. Phys.* **52**, 063001 (2019).
- [7] M. Weisheit, S. Fähler, A. Marty, Y. Souche, C. Poinsignon, and D. Givord, Electric field-induced modification of magnetism in thin-film ferromagnets, *Science* **315**, 349 (2007).
- [8] T. Maruyama, Y. Shiota, T. Nozaki, K. Ohta, N. Toda, M. Mizuguchi, A. Tulapurkar, T. Shinjo, M. Shiraishi, S. Mizukami, Y. Ando, and Y. Suzuki, Large voltage-induced magnetic anisotropy change in a few atomic layers of iron, *Nat. Nanotechnol.* **4**, 158 (2009).
- [9] P. K. Amiri, J. G. Alzate, X. Q. Cai, F. Ebrahimi, Q. Hu, K. Wong, C. Grèzes, H. Lee, G. Yu, X. Li, M. Akyol, Q. Shao, J. A. Katine, J. Langer, B. Ocker, and K. L. Wang, Electric-



- field-controlled magnetoelectric RAM: Progress, challenges, and scaling, *IEEE Trans. Magn.* **51**, 3401507 (2015).
- [10] C. Song, B. Cui, F. Li, X. Zhou, and F. Pan, Recent progress in voltage control of magnetism: Materials, mechanisms, and performance, *Prog. Mater. Sci.* **87**, 33 (2017).
- [11] S. Miwa, M. Suzuki, M. Tsujikawa, K. Matsuda, T. Nozaki, K. Tanaka, T. Tsukahara, K. Nawaoka, M. Goto, Y. Kotani, T. Ohkubo, F. Bonell, E. Tamura, K. Hono, T. Nakamura, M. Shirai, S. Yuasa, and Y. Suzuki, Voltage controlled interfacial magnetism through platinum orbits, *Nat. Commun.* **8**, 15848 (2017).
- [12] C. G. Duan, J. P. Velev, R. F. Sabirianov, Z. Zhu, J. Chu, S. S. Jaswal, and E. Y. Tsymlal, Surface Magnetoelectric Effect in Ferromagnetic Metal Films, *Phys. Rev. Lett.* **101**, 137201 (2008).
- [13] M. Tsujikawa and T. Oda, Finite Electric Field Effects in the Large Perpendicular Magnetic Anisotropy Surface Pt/Fe/Pt(001): A First-Principles Study, *Phys. Rev. Lett.* **102**, 247203 (2009).
- [14] K. Nakamura, R. Shimabukuro, Y. Fujisawa, T. Akiyama, T. Ito, and A. J. Freeman, Giant Modification of the Magnetocrystalline Anisotropy in Transition-Metal Monolayers by an External Electric Field, *Phys. Rev. Lett.* **102**, 187201 (2009).
- [15] P. V. Ong, N. Kioussis, D. Odkhuu, P. K. Amiri, K. L. Wang, and G. P. Carman, Giant voltage modulation of magnetic anisotropy in strained heavy metal/magnet/insulator heterostructures, *Phys. Rev. B* **92**, 020407(R) (2015).
- [16] F. Ibrahim, H. X. Yang, A. Hallal, B. Dieny, and M. Chshiev, Anatomy of electric field control of perpendicular magnetic anisotropy at Fe/MgO interfaces, *Phys. Rev. B* **93**, 014429 (2016).
- [17] T. Kawabe, K. Yoshikawa, M. Tsujikawa, T. Tsukahara, K. Nawaoka, Y. Kotani, K. Toyoki, M. Goto, M. Suzuki, T. Nakamura, M. Shirai, Y. Suzuki, and S. Miwa, Electric-field-induced changes of magnetic moments and magnetocrystalline anisotropy in ultrathin cobalt films, *Phys. Rev. B* **96**, 220412(R) (2017).
- [18] A. A. Tulapurkar, Y. Suzuki, A. Fukushima, H. Kubota, H. Maehara, K. Tsunekawa, D. D. Djayaprawira, N. Watanabe, and S. Yuasa, Spin-torque diode effect in magnetic tunnel junctions, *Nature (London)* **438**, 339 (2005).
- [19] J. C. Sankey, P. M. Braganca, A. G.F. Garcia, I. N. Krivorotov, R. A. Buhrman, and D. C. Ralph, Spin-Transfer-Driven Ferromagnetic Resonance of Individual Nanomagnets, *Phys. Rev. Lett.* **96**, 227601 (2006).
- [20] T. Nozaki, Y. Shiota, S. Miwa, S. Murakami, F. Bonell, S. Ishibashi, H. Kubota, K. Yakushiji, T. Saruya, A. Fukushima, S. Yuasa, T. Shinjo, and Y. Suzuki, Electric-field-induced ferromagnetic resonance excitation in an ultrathin ferromagnetic metal layer, *Nat. Phys.* **8**, 491 (2012).
- [21] F. Bonell, Y. T. Takahashi, D. D. Lam, S. Yoshida, Y. Shiota, S. Miwa, T. Nakamura, and Y. Suzuki, Reversible change in the oxidation state and magnetic circular dichroism of Fe driven by an electric field at the FeCo/MgO interface, *Appl. Phys. Lett.* **102**, 152401 (2013).
- [22] G. Radaelli, D. Petti, E. Plekhanov, I. Fina, P. Torelli, B. R. Salles, M. Contoni, C. Rinaldi, D. Gutiérrez, G. Panaccione, M. Varela, S. Picozzi, J. Fontcuberta, and R. Bertacco, Electric control of magnetism at the Fe/BaTiO<sub>3</sub> interface, *Nat. Commun.* **5**, 3404 (2014).
- [23] C. Bi, Y. Liu, T. Newhouse-Illige, M. Xu, M. Rosales, J. W. Freeland, O. Mryasov, S. Zhang, S. G. E. te Velthuis, and W. G. Wang, Reversible Control of Co Magnetism by Voltage-Induced Oxidation. *Phys. Rev. Lett.* **113**, 267202 (2014).
- [24] B. Cui, C. Song, G. A. Gehring, F. Li, G. Wang, C. Chen, J. Peng, H. Mao, F. Zeng, and F. Pan, Electrical manipulation of orbital occupancy and magnetic anisotropy in manganites, *Adv. Func. Mater.* **25**, 864 (2015).
- [25] A. Koziol-Rachwał, T. Nozaki, V. Zayets, H. Kubota, A. Fukushima, S. Yuasa, and Y. Suzuki, The effect of the MgO buffer layer thickness on magnetic anisotropy in MgO/Fe/Cr/MgO buffer/MgO(001), *J. Appl. Phys.* **120**, 085303 (2016).
- [26] C.-H. Lambert, A. Rajanikanth, T. Hauet, S. Mangin, and E. E. Fullerton, Quantifying perpendicular magnetic anisotropy at the Fe-MgO(001) interface, *Appl. Phys. Lett.* **102**, 122410 (2013).
- [27] K. Tanaka, S. Miwa, Y. Shiota, M. Mizuochi, T. Shinjo, and Y. Suzuki, Large voltage-induced magnetic anisotropy field change in ferrimagnetic FeGd, *Appl. Phys. Express* **8**, 073007 (2015).
- [28] S. Miwa, J. Fujimoto, P. Risius, K. Nawaoka, M. Goto, and Y. Suzuki, Strong Bias Effect on Voltage-Driven Torque at Epitaxial Fe-MgO Interface, *Phys. Rev. X* **7**, 031018 (2017).
- [29] T. Nakamura, T. Muro, F. Z. Guo, T. Matsushita, T. Wakita, T. Hirono, Y. Takeuchi, and K. Kobayashi, Development of a soft X-ray magnetic circular dichroism spectrometer using a 1.9 T electromagnet at BL25SU of SPring-8, *J. Electron Spectrosc. Relat. Phenom.* **144–147**, 1035 (2005).
- [30] T. Hirono, H. Kimura, T. Muro, Y. Saitoh, and T. Ishikawa, Full polarization measurement of SR emitted from twin helical undulators with use of Sc/Cr multilayers at near 400 eV, *J. Electron Spectrosc. Relat. Phenom.* **144–147**, 1097 (2005).
- [31] L. Tröger, D. Arvanitis, K. Baberschke, H. Michaelis, U. Grimm, and E. Zschech, Full correction of the self-absorption in soft-fluorescence extended x-ray-absorption fine structure, *Phys. Rev. B* **46**, 3283 (1992).
- [32] B. T. Thole, P. Carra, F. Sette, and G. van der Laan, X-ray Circular Dichroism as a Probe of Orbital Magnetization. *Phys. Rev. Lett.* **68**, 1943 (1992).
- [33] P. Carra, B. T. Thole, M. Altarelli, and X. Wang, X-ray Circular Dichroism and Local Magnetic Fields, *Phys. Rev. Lett.* **70**, 694 (1993).
- [34] C. T. Chen, Y. U. Idzerda, H. J. Lin, N. V. Smith, G. Meigs, E. Chaban, G. H. Ho, E. Pellegrin, and F. Sette, Experimental Confirmation of the X-Ray Magnetic Circular Dichroism Sum Rules for Iron and Cobalt, *Phys. Rev. Lett.* **75**, 152 (1995).
- [35] P. Srivastava, N. Haack, H. Wende, R. Chauvistré, and K. Baberschke, Modification of the electronic structure of Ni/Cu(001) as a function of the film thickness, *Phys. Rev. B* **56**, R4398 (1997).
- [36] Y. Suzuki and S. Miwa, Magnetic anisotropy of ferromagnetic metals in low-symmetry systems, *Phys. Lett A* **383**, 1203 (2019).